A New Series of Magnetic Rare Earth Cuprates: RCu_2O_4 (R = La, Nd, Sm, and Eu)

Steven W. Keller,[†,§] Virginia A. Carlson,[‡,§] David Sandford,[§] Frauke Stenzel,[§] Angelica M. Stacy,*[,§] George H. Kwei,[⊥] and Miguel Alario-Franco[∥]

Contribution from the Department of Chemistry, University of California, Berkeley, Berkeley, California 94720-9989, Los Alamos National Laboratory, Los Alamos, New Mexico 87545, and Facultad Ciencias Quimicas, Universidad Complutense, 28040 Madrid, Spain

Received February 28, 1994[●]

Abstract: The synthesis, crystal structure, and magnetic properties of a new series of isostructural rare earth cuprates, RCu_2O_4 (R = La, Nd, Sm, and Eu), are reported. The highly oxidized materials with an average formal copper oxidation state of $Cu^{2.5+}$ were isolated by precipitation from molten NaOH at 400 °C. Powder X-ray diffraction data for $EuCu_2O_4$ combined with neutron diffraction data for $NdCu_2O_4$ were used to determine the crystal structure and refine the structure by Rietveld profile analysis. The lattice parameters for $NdCu_2O_4$ in the non-standard monoclinic space group $I2/a$ derived from the neutron data set are the following: a = 5.826(1) Å, b = 9.703(1) Å, c = 5.753(1) Å, and β = 92.341(1)°. The copper–oxygen network consists of a three-dimensional array of CuO_4 distorted square planes that are cornered-shared; the Cu–O–Cu bond angle is ~115°. These phases exhibit magnetic ordering of the copper spins as determined by a large increase in the magnetization as the temperature is lowered, the onset of which varies between 18 and 28 K, depending on R. While the negative Weiss constants for $LaCu_2O_4$ and $NdCu_2O_4$ indicate that the predominant interaction is antiferromagnetic, the saturation moments of ~0.13 μ_B per mol of RCu_2O_4 indicate that there is a significant ferromagnetic component, possibly due to canting of the ordered copper moments.

Introduction

The formal oxidation state of copper is non-integral, but near Cu^{2+}, in the several classes of copper oxide phases that are high-temperature superconductors.[1] For example, phases partially oxidized to $Cu^{(2+x)+}$ (e.g., $La_{2-x}Sr_xCuO_4$ for $0.05 < x < 0.30$)[2] or partially reduced to $Cu^{(2-x)+}$ (e.g., $Nd_{2-x}Ce_xCuO_4$ for $x \sim 0.15$)[3] are *metallic* conductors at room temperature and exhibit superconductivity near 30 K; magnetic ordering of the copper moments is not observed. However, in the corresponding *insulating* parent materials (La_2CuO_4 and Nd_2CuO_4) in which the formal copper oxidation state is Cu^{2+}, antiferromagnetic ordering of the copper moments is observed instead of superconductivity.[4] A transition from antiferromagnetism to superconductivity is also observed as a function of composition for $YBa_2Cu_3O_{7-\delta}$; while superconductivity is observed for δ near 0 (non-integral formal copper oxidation state), antiferromagnetic order is observed for δ = 1 (formal copper oxidation state of Cu^{2+}).[5] We are interested in probing further this interplay between valence, magnetic order, and superconductivity by varying the formal oxidation state of the copper, as well as the connectivity of the copper–oxygen network, through the synthesis of new classes of cuprates.

The copper oxides that exhibit superconductivity are related structurally to one another in that they all contain layers of corner-sharing CuO_4 units which are approximately square planar.[6] In some of these phases there are one or two additional bonds to oxygen above and/or below the layers; these axial bonds are typically longer than the Cu–O bonds within the layers. Here we report the synthesis of a new class of copper oxides, RCu_2O_4 (R = La, Nd, Sm, Eu), with a distinct copper–oxygen network in which planar CuO_4 units are corner-shared in a three-dimensional array; this is the first example of such connectivity in a cuprate. These phases were prepared by precipitation from molten NaOH at 400 °C by slightly modifying the preparation reported for the synthesis of $La_{2-x}(Na,K)_xCuO_4$ from molten hydroxide.[7,8,9]

Antiferromagnetic coupling between copper spins is observed typically in materials containing copper in a formal oxidation state of Cu^{2+}. Exceptions are the copper halides, A_2CuX_4 (A = K, Rb, or NH_4; X = Cl or Br),[10] and the recently synthesized oxide, $La_4Ba_2Cu_2O_{10}$,[11] which both exhibit ferromagnetic order below 2 and ~5 K, respectively. In contrast, copper oxides with non-integral oxidation states near Cu^{2+} are non-magnetic, as are oxides of both Cu^+ and Cu^{3+}.[12] Here we report unusual and complex magnetic behavior in RCu_2O_4. With copper in a non-

* Author to whom correspondence should be addressed.
† Current address: Department of Chemistry, The Pennsylvania State University, University Park, PA 16802.
‡ Current address: Rohm and Haas Research Laboratories, 727 Norristown Road, Box 904, Spring House, PA 19477-0904.
§ University of California.
⊥ Los Alamos National Laboratory.
∥ Universidad Complutense.
● Abstract published in *Advance ACS Abstracts,* August 1, 1994.

(1) See, for example: Sleight, A. W. In *Chemistry of High-Temperature Superconductors*; Nelson, D. L., Wittingham, M. S., George, T. F., Eds.; American Chemical Society: Washington, DC, 1987; ACS Symp. Ser. No. 351, pp 2–12.
(2) Bednorz, J. G.; Müller, K. A. *Z. Phys.* **1986**, *B64*, 189.
(3) (a) Tokura, Y.; Takagi, H.; Uchida, S. *Nature* **1989**, *337*, 345. (b) Markert, J. T.; Maple, M. B. *Solid State Commun.* **1989**, *70*, 145.
(4) (a) Luke, G. M.; Lee, L. P.; Sternleib, B. J.; Uemura, Y. J.; Brewer, J. H.; Kodono, R.; Kiefl, R. F.; Kreitzman, S. R.; Riseman, T. M.; Stronach, C. E.; Davis, M. R.; Uchida, S.; Takagi, H.; Hidaka, Y.; Muakami, T.; Gopalakrishnan, J.; Sleight, A. W.; Subramanian, M. A.; Early, E. A.; Markert, J. T.; Maple, M. B.; Seaman, C. L. *Phys. Rev. B* **1990**, *42*, 7981. (b) Uemura, Y. T.; Kossler, W. J.; Yu, X. H.; Kempton, J. R.; Schone, H. E.; Opie, D.; Stronach, C. E.; Johnston, D. C.; Alvarez, M. S.; Goshorn, D. P. *Phys. Rev. Lett.* **1987**, *59*, 1045.
(5) Tranquada, J. M.; Moudden, A. H.; Goldman, A. I.; Zolliker, P.; Cox, D. E.; Shirane, G.; Sinha, S. K.; Vaknin, D.; Johnson, D. C.; Alvarez, M. S.; Jacobson, A. J.; Lewandowski, J. T.; Newsam, J. M. *Phys. Rev. B* **1988**, *38*, 2477.
(6) Beno, M. A.; Soderholm, L.; Capone, D. W., II; Hinks, D. G.; Jorgenson, J. D.; Grace, J. D.; Schuller, I. K. *Appl. Phys. Lett.* **1987**, *51*, 57.
(7) Ham, W. K.; Holland, G. F.; Stacy, A. M. *J. Am. Chem. Soc.* **1988**, *110*, 5214.
(8) Günther, W.; Schöllhorn, R. *Physica C* **1992**, *203*, 115–120.
(9) Stoll, S.; Torardi, C. C.; Stacy, A. M. *Inorg. Chem.* **1994**, *33*, 2761.
(10) Carlin, R. L. In *Magnetochemistry*; Springer-Verlag: Berlin, 1986; p 143.
(11) Mizuno, F.; Masuda, H.; Hirabayashi, I.; Tanaka, S.; Hasegawa, M.; Mizutani, U. *Nature* **1990**, *345*, 788.

0002-7863/94/1516-8070$04.50/0

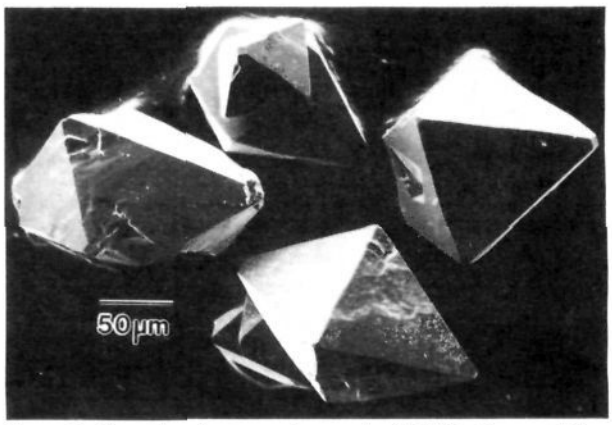

Figure 1. Scanning electron micrograph of $NdCu_2O_4$ crystallites. Accelerating voltage was 20 keV; the scale is shown by the 50 μm bar.

integral, formal oxidation state of $Cu^{2.5+}$, these phases are more highly oxidized than the copper oxides that exhibit superconductivity. It is notable that these new phases exhibit magnetic order even though the average oxidation state is distinct from Cu^{2+}, with a net increase in magnetization below ca. 30 K.

Experimental Section

Synthesis. All reagents were used without further treatment or purification. After 20 g of NaOH (Fisher 98%) was melted and dehydrated in a silver crucible at 400 °C for 12–24 h in air, 0.342 mmol of R_2O_3 (La_2O_3, Aldrich 99.99%; Nd_2O_3 and Eu_2O_3, Alfa Products 99.9%; Sm_2O_3, Aldrich 99.9%) and 1.37 mmol of CuO (Fisher 98%) were added. Prior to addition, these two reagents were ground together to dryness with acetone. The mixture was reacted for approximately 48 h at 400 °C. Upon completion of the reaction, a black precipitate was visible at the bottom and on the sides of the crucible and the molten hydroxide flux had turned pale green. The flux was decanted, and the crucible quenched into cold water. The remaining hydroxide was dissolved with flowing distilled water. The shiny, black, pseudo-octahedral-shaped crystallites (shown in Figure 1) were collected by vacuum filtration, washed with distilled water followed by acetone, and finally dried in air at 130 °C for several hours.

In some instances, CuO, R_2CuO_4, and/or $NaCuO_2$ impurities were detected by X-ray diffraction. These phases can be removed by washing the product in 6 M HCl with no adverse affects to the RCu_2O_4 crystallites. We note that unfortunately the washing of the rather large sample used for neutron diffraction was inadequate and a CuO impurity remained (~14 wt %). Since collecting the neutron diffraction data, we have found that it is possible to avoid the synthesis of these impurity phases by flowing air with 80% relative humidity over the reaction mixture. Alternatively, the reaction can be carried out in a NaOH/KOH eutectic melt at 350 °C instead of in NaOH at 400 °C, and pure RCu_2O_4 can be obtained.

Wavelength Dispersive Spectroscopy. Crystallites were mounted in Al cylinders filled with epoxy. The cylinder ends were polished first with sandpaper and finally with diamond paste to expose clean level surfaces to the electron beam. Samples then were coated with carbon film and loaded into an eight-spectrometer ARL SEMQ Microprobe instrument; wavelengths accessible with this instrument were in the range $0.707 \leq \lambda \leq 135.9$ Å. A 15.0 keV incident beam energy was used with a 10 s acquisition time for each data point. A variety of standard metals and oxides were analyzed to account for channel detector and electronic dead time, beam current drift, and standard drift in real time.[13] Assuming the copper stoichiometry to be 2.0, the atomic ratios for R:Cu:O were 0.94(2):2.0:4.12(4) and 0.97(1):2.0:4.13(3) for R = Sm and Eu, respectively. The sodium content of all the crystallites was <0.02%.

X-ray Diffraction. A Siemens D500 diffractometer equipped with a position-sensitive detector and a quartz-crystal incident beam monochromator (Cu $K\alpha_1$ only; $\lambda = 1.5404$ Å) was used to collect a diffraction pattern for $EuCu_2O_4$. Diffraction data were obtained in the range $10° \leq 2\theta \leq 100°$ by using a step size of 0.05° 2θ and a 5 s counting time. Si powder was used as an internal standard; typically the (111), (220), and (310) Bragg reflections from Si were observed. Additional diffraction patterns for the other isostructural phases were collected on another Siemens D500 diffractometer using Cu $K\alpha$ radiation (no incident beam monochromator). Si powder was again used as an internal standard. Data were collected in the range $10° \leq 2\theta \leq 80°$. Step sizes were typically 0.04° 2θ and counting times varied between 3 and 5 s depending on sample crystallinity.

Neutron Diffraction. A neutron diffraction pattern for $NdCu_2O_4$ was collected on the general purpose powder diffractometer (GPPD) with incident neutrons produced at the intense pulsed neutron source at the Argonne National Laboratory. The Nd sample was chosen due to its low neutron absorption cross-section as compared to the other lanthanide ions. Approximately 2 g of $NdCu_2O_4$ were packed into a vanadium can and placed in the diffractometer. Room-temperature data were collected in six detector banks (± 150°, ± 90°, and ± 60°) for 4 h at a proton current of 14 mA.

Resistivity Measurements. For qualitative resistivity measurements, a small amount of poly(tetrafluoroethylene) was ground together with RCu_2O_4 powder and the mixture was pressed into a 0.5 in. diameter pellet (ca. 2 mm thick). Gold leads were attached to opposite sides of the pellet with silver paint. The resistance across the pellet was then measured with a multimeter in air (296 K) and while immersed in liquid nitrogen (77 K).

Magnetic Measurements. A Quantum Design SQUID magnetometer was used for all magnetic measurements. Field calibration ($H < 100$ G) was done by measuring the magnetization of a superconducting Sn sphere at 2 K. As the diamagnetic contributions from the poly(chlorotrifluoroethylene) (Kel-F) container were more than 10^3 times smaller than the sample magnetizations in the low-field measurements no container corrections were made. For high-field data, the magnetizations of the empty containers were subtracted from the total measured magnetizations, and the diamagnetic core contributions were subtracted from the calculated susceptibilities. Because of the very small signal from $LaCu_2O_4$ a special container was used; an Al cylinder was fitted inside a Teflon outer container, so as to cancel out as much of the container diamagnetism as possible.[14] In this way the measured magnetizations never change sign during the duration of the experiment, and the data are less erratic. Unless otherwise stated, all magnetic data were collected by cooling the sample from high to low temperature.

Structure Refinement and Solution

Accurate peak positions in the X-ray diffraction pattern of $EuCu_2O_4$ ($\lambda_{ave} = 1.5418$ Å) were determined by using a peak-profile fitting program.[15] After a zero-point correction based on the Si peak positions was applied, the data were used as input for the auto-indexing program ITO.[16] The data were indexed satisfactorily to a monoclinic cell. The systematic absence $h + k + l = 2n + 1$ was observed, consistent with body-centered translational symmetry. Inspection of the other RCu_2O_4 (R = La, Nd, and Sm) diffraction patterns indicated that they were isostructural with $EuCu_2O_4$.

The solution of the structure was begun in the most symmetric of the possible space groups, $I2/a$;[17] this choice was confirmed by successful refinement of the structure. The positions of the heavy atoms were obtained from the X-ray diffraction data by Patterson methods and refined by using the GSAS software package.[18] Although the oxygen atom positions were difficult to determine and refine from the X-ray diffraction data, reasonable estimates were obtained by trial and error.

Refinement of the neutron diffraction data collected for $NdCu_2O_4$ confirmed the locations of the heavy atoms and slightly repositioned the oxygen atoms. Since CuO was present as an impurity in the sample used to collect the neutron diffraction data, a two-phase refinement was done by the Rietveld method, again by using the GSAS software package. No regions of the pattern were excluded from the refinement. A seven-term Fourier series was used to describe the background. Initially, a two-phase refinement was performed on the data ranging from $d = 0.40$ to

(12) (a) Goodenough, J. B.; Demazeau, G.; Pouchard, M.; Hagenmüller, P. *J. Solid State Chem.* **1973**, *8*, 325. (b) Arjomand, M.; Machin, D. J. *J. Chem. Soc., Dalton Trans.* **1975**, 1061.

(13) Armstrong, J. T. In *Microbeam Analysis–1988*; Newbury, D. E., Ed.; Proceedings of the 23rd Annual Conference of the Microbeam Analysis Society, San Francisco, CA, 1988; pp 239–246.

(14) For design and construction specifics of this container see: VerNooy, P. D. Ph.D. Thesis, University of California, Berkeley, March 1991.

(15) Siemens DIFFRAC-AT Software Package, 1986, SOCABIM.

(16) Visser, J. W. *J. Appl. Crystallogr.* **1969**, *2*, 89.

(17) The non-standard, body-centered monoclinic space group was chosen so as to make the β-angle close to 90°, and therefore aid in viewing the structure.

(18) Larson, A. C.; Von Dreele, R. B. Los Alamos Report, LAUR 86-748, 1986, Los Alamos National Laboratory, U.S.A.

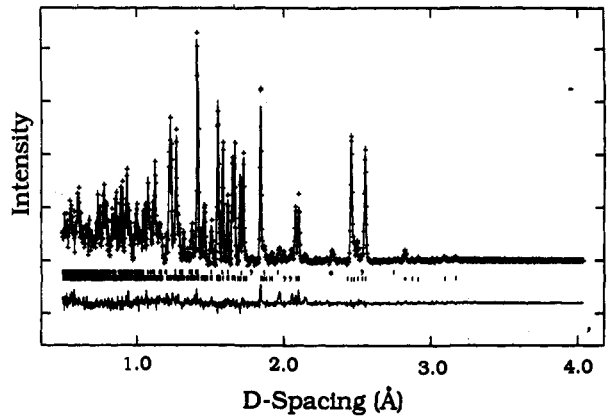

Figure 2. Powder neutron diffraction pattern for $NdCu_2O_4$. The crosses are the data points and the line through them is the calculated profile from Rietveld refinements. The upper set of tick marks below the data indicate positions of expected reflections for CuO and the lower set are those for $NdCu_2O_4$. The lower curve is the difference between the observed and calculated profiles (the scale is the same as for the observed profile).

Table 1. Structural Parameters and Agreement Factors for Neutron Diffraction Refinement of $NdCu_2O_4$[a]

space group	$I2/a$
a (Å)	5.826(1)
b (Å)	9.703(1)
c (Å)	5.753(1)
β (deg)	92.341(1)
no. of background parameters	7
no. of profile parameters	5
R_p	3.23
R_{wp}	4.58
R_E	2.79
χ^2	1.642

[a] $R_p = 100\Sigma|y_{io} - (1/c)y_{ic}|/\Sigma|y_{io}|$, $R_{wp} = 100(\Sigma w\{y_{io} - (1/c)y_{ic}\}^2/\Sigma w\{y_{io}\}^2)^{1/2}$, $R_E = 100\{(N - P + C)/w(y_{io})^2\}^{1/2}$, $\chi^2 = (R_{wp}/R_E)^2$, where y_i is an independent observation, P is the number of least-squares parameters, and C is the number of constraint functions.

Table 2. Positional and Isotropic Thermal Parameters for $NdCu_2O_4$ and Their Estimated Standard Deviations

	atom	x	y	z	occu	$U_{(iso)}$ (Å^2)
4e	Nd(1)	0.25	0.125(1)	0	1.07(1)	0.59(4)
4c	Cu(1)	0.75	0.25	0.75	1.00	0.75(4)
4b	Cu(2)	0	0.5	0	1.00	0.40(4)
8f	O(1)	0.5303(3)	0.8254(2)	0.6319(3)	0.98(1)	0.56(4)
8f	O(2)	0.9002(3)	0.0712(2)	0.2155(3)	0.96(1)	0.62(4)

5.32 Å to account for the 14 wt % CuO impurity. Lattice constants, atomic positions, isotropic thermal parameters and oxygen occupancies for $NdCu_2O_4$, and lattice constants and atomic positions for CuO were refined. Peak profiles were refined by using a pseudo-Voigtian function, including a linear Gaussian term, two nonlinear Lorentzian terms, and an asymmetric contribution; the atom positions were then allowed to vary. In addition, nonstructural parameters such as background, scale, sample absorption, and peak profiles (including isotropic strain broadening) were also fit.

The neutron diffraction data for $NdCu_2O_4$ (crosses), the fit corresponding to the final model (solid line), and the difference between the two (lower curve), as well as the positions of expected Bragg reflections (tick marks), are displayed in Figure 2. The final structural parameters and agreement factors from this fit are listed in Table 1. Positional parameters for all of the atoms, their refined occupancy, and isotropic thermal parameters are given in Table 2. A list of selected bond lengths and bond angles for $NdCu_2O_4$ is located in Table 3. For the three other isotypic phases, a least-squares fit of not less than 19 X-ray reflections yielded the lattice parameters and average discrepancies shown in Table 4.

Results and Discussion

Synthesis. Previously, it has been shown that molten NaOH and KOH can be used to prepare samples of $La_{2-x}(Na,K)_xCuO_4$,[7,8] including single crystals,[9] which exhibit superconductivity. For the synthesis of these phases, the reactant metal oxides (CuO and La_2O_3) are dissolved in hydroxide fluxes containing large amounts of dissolved water (acidic fluxes) via the following reaction, written for the general case of the dissolution of a metal oxide (MO):[19]

$$MO_{(solid)} + H_2O_{(solution)} \leftrightarrow M^{(2)+}{}_{(solution)} + 2OH^-$$

As the flux is dried at temperatures above 300 °C, this reaction shifts back to the left causing (mixed) metal oxides to precipitate from solution.

Here we have heated NaOH (or the NaOH/KOH eutectic) in air to remove water before adding the reactant metal oxides (CuO and La_2O_3), and the more-highly-oxidized product, $LaCu_2O_4$, was isolated instead of $La_{2-x}(Na,K)_xCuO_4$. Previous work has shown that O_2 reacts to a greater extent with melts that have a lower water content to form O_2^- and/or O_2^{2-}, thus increasing the oxidizing potential of the melt.[20] As a result, after slow dissolution of the reactant metal oxides, the more highly oxidized phase $LaCu_2O_4$ is precipitated. We note that this low-temperature solution route allows for the growth of large crystallites; however, in the present case, crystals suitable for single-crystal X-ray diffraction experiments were not formed.

$NdCu_2O_4$, $SmCu_2O_4$, and $EuCu_2O_4$ can be isolated upon replacing La_2O_3 with the appropriate rare earth oxide. It is noteworthy that neither the Ce nor the Pr analogs of RCu_2O_4 could be prepared under these conditions. Presumably, the tetravalent oxidation state of these two lanthanides would be favored in the highly oxidizing environment of the molten alkali metal hydroxides. Additionally, we have prepared $GdCu_2O_4$, $DyCu_2O_4$, and YCu_2O_4 but do not report further on their properties here.[21]

It appears that molten alkali metal hydroxides provide a special environment that is necessary for the synthesis of these highly oxidized phases. Our attempts to prepare RCu_2O_4 by direct reaction of the binary oxides, CuO and R_2O_3, in air have led to the isolation of CuO and R_2CuO_4.[21] We propose that dissolved

Table 3. Selected Bond Distances and Bond Angles for $NdCu_2O_4$

atom 1–atom 2	distance (Å)	atom 1–atom 2	distance (Å)
Nd(1)–Nd(1)	3.791(1) (×2)	Nd(1)–O(2)	2.416(2) (×2)
Nd(1)–Nd(1)	3.763(1) (×2)	Cu(1)–Cu(1)	2.876(1) (×2)
Nd(1)–Cu(1)	3.517(1) (×2)	Cu(2)–Cu(2)	2.913(1) (×2)
Nd(1)–Cu(1)	3.418(1) (×2)	Cu(1)–Cu(2)	3.201(2) (×2)
Nd(1)–Cu(2)	3.494(1) (×2)	Cu(1)–Cu(2)	3.147(2) (×2)
Nd(1)–Cu(2)	3.395(1) (×2)	Cu(1)–O(1)	1.938(2) (×2)
Nd(1)–O(1)	2.477(2) (×2)	Cu(1)–O(2)	1.957(2) (×2)
Nd(1)–O(1)	2.465(2) (×2)	Cu(2)–O(1)	1.861(2) (×2)
Nd(1)–O(2)	2.484(2) (×2)	Cu(2)–O(2)	1.848(2) (×2)

atom 1–atom 2–atom 3	angle (deg)	atom 1–atom 2–atom 3	angle (deg)
O(1)–Cu(1)–O(1)	180.0(1)	O(1)–Cu(2)–O(2)	92.41(1)
O(1)–Cu(2)–O(1)	180.0(1)	O(2)–Cu(1)–O(2)	180.0(1)
O(1)–Cu(1)–O(2)	95.02(1)	O(2)–Cu(2)–O(2)	180.0(1)
O(1)–Cu(1)–O(2)	84.98(1)	Cu(1)–O(1)–Cu(2)	114.80(1)
O(1)–Cu(2)–O(2)	87.60(1)	Cu(1)–O(2)–Cu(2)	111.55(1)

Table 4. Lattice Parameters for RCu_2O_4; Space Group $I2/a$

R	a (Å)	b (Å)	c (Å)	β (deg)	vol (Å^3)
La[a]	5.919(1)	9.764(2)	5.846(1)	92.24(1)	337.6
Nd[b]	5.826(1)	9.703(1)	5.753(1)	92.341(1)	324.6
Sm[a]	5.784(1)	9.667(1)	5.707(1)	92.42(1)	318.8
Eu[a]	5.762(1)	9.646(2)	5.684(1)	92.40(1)	315.6

[a] From least-squares fit of not less than 19 indexed X-ray Bragg reflections. [b] From neutron diffraction profile refinement.

(19) Plembeck, J. A. In *Encyclopedia of Electrochemistry of the Elements*, Bard, A. J., Ed.; Fused Salt Systems, Vol. X; Marcel Dekker, Inc.: New York (1976), pp 285–9.
(20) Goret, J.; Tremillion, B. *Bull. Chim. Soc. Fr.* **1965**, 67.
(21) Keller, S. W. Ph.D. Dissertation, University of California–Berkeley, 1991.

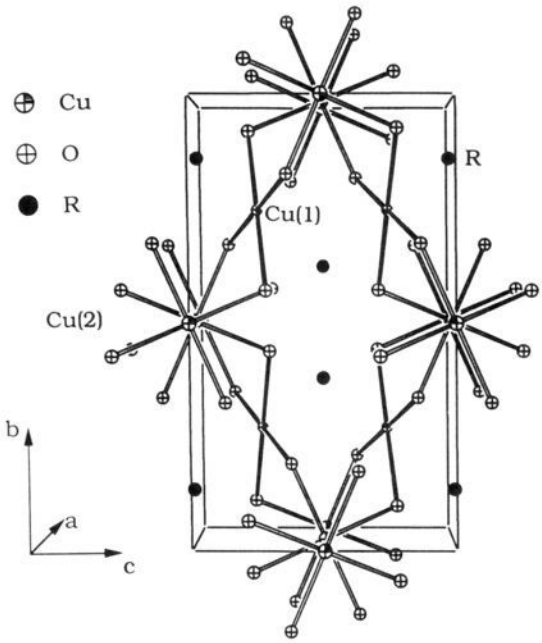

Figure 3. ORTEP diagram of the RCu_2O_4 unit cell viewed down the *a*-axis. R–O bonds are omitted for clarity. Thermal ellipsoids represent 50% probability.

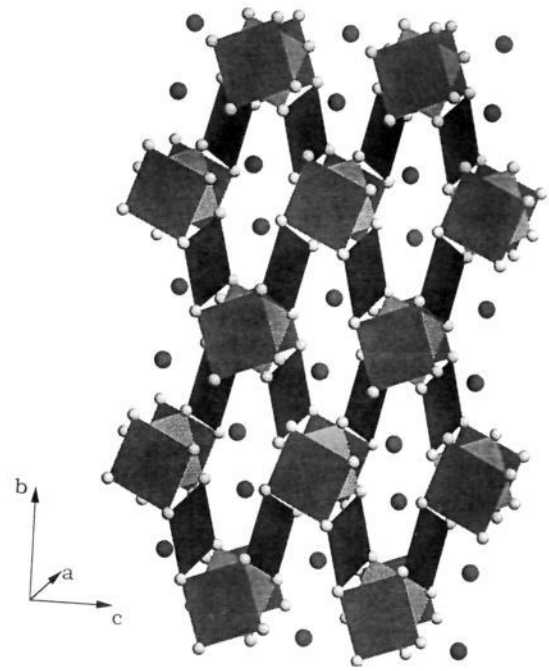

Figure 4. A view down the *a*-axis of RCu_2O_4 showing the Cu–O coordination polyhedra with oxygen atoms at the corners and the copper atoms not shown. The light and medium gray $Cu(2)O_4$ units (shading is alternated for clarity) form staggered stacks perpendicular to the plane of the page. Connecting these stacks into a three-dimensional array are the dark gray $Cu(1)O_4$ units, each a part of a similar stack that is parallel to the plane of the page. Rare earth cations are the large gray atoms between the stacks.

oxygen in the form of O_2^- and/or O_2^{2-} in the hydroxide flux allows for the oxidation of Cu^{2+} to Cu^{3+}. Additionally, we note that the RCu_2O_4 phases decompose in air above ~700 °C to CuO, R_2CuO_4, and O_2.

Structure. A view of the monoclinic unit cell of RCu_2O_4 with the *a* axis nearly perpendicular to the plane of the page is shown in Figure 3 (the R–O bonds are omitted for clarity). There are two crystallographically distinct sites for copper in the unit cell (shown as partially shaded circles, and labeled Cu(1) and Cu(2)), two distinct sites for oxygen (both shown as small circles containing crosses), and one unique site for the rare earth atom (shown as a filled black circle). Each copper atom is surrounded by four oxygen atoms in a distorted square-planar arrangement, and the CuO_4 units are corner-shared in a three-dimensional array. The oxygen atoms are each bonded to two rare-earth atoms and two copper atoms with pseudo-tetrahedral geometry. The rare-earth atoms each share eight oxygen atoms with the $[Cu_2O_4]^{3-}$ network.

A second view of the structure with several unit cells included is shown in Figure 4. In this figure, the CuO_4 units are depicted as squares (slightly irregular) with the oxygen atoms (small spheres) at the corners and the copper atoms omitted. The rare-earth atoms are shown as the large spheres. The two crystallographically distinct sites for copper are differentiated by the shading with the darkest shading for $Cu(1)O_4$ units and the two different lighter shadings for $Cu(2)O_4$ units. The sharp angle of the $Cu(1)O_4$ units with respect to the plane of the $Cu(2)O_4$ units is evident.

The three-dimensional network formed by the CuO_4 units can be described as follows. As shown in Figures 3 and 4, there exists a stack of $Cu(2)O_4$ units parallel to the *a*-axis. Each is rotated roughly 45° with respect to its neighbors along the stack. No direct bonding (i.e. no Cu(2)–Cu(2) bonds) exists between the units that comprise this stack; the Cu(2)–Cu(2) distance between adjacent units is ~2.9 Å. Instead, the $Cu(2)O_4$ units are bridged via four different Cu(1) atoms that are themselves pieces of $Cu(1)O_4$ units that form similar stacks parallel to the *c*-axis. A side view of the $Cu(2)O_2$ stacks is shown in Figure 5 where now the $Cu(1)O_2$ stacks recede into the page.

The average Cu–O bond lengths and the O–Cu–O bond angles are quite different for Cu(1) and Cu(2) as indicated in Table 3. Both copper atoms are bonded to two O(1) and two O(2) atoms. The average Cu(2)–O distance of 1.85 Å is 0.1 Å shorter than the average Cu(1)–O bond length of 1.95 Å. This latter value is typical for copper in a formal oxidation state of Cu^{2+} (e.g. in CuO: Cu–O = 1.96 Å) while the shorter distance is found for Cu^{3+} (e.g. in $Ba_4NaCuO_4(CO_3)_2$: Cu–O = 1.85 Å[22]). The distortion from ideal square-planar coordination is larger for Cu(1) with O–Cu(1)–O angles of 85° and 95°, as compared with O–Cu(2)–O angles of 87.6° and 92.4°. The indication of two distinct oxidation states is consistent with the stoichiometry of the material derived from microprobe analysis (i.e., one Cu^{2+} and one Cu^{3+} per formula unit).

The rare-earth atoms are located in a distorted square antiprismatic array of oxygen atoms (four O(1) and four O(2) atoms); the Nd–O bond lengths vary between 2.416 and 2.484 Å. The closest Nd–Nd distance is 3.763 Å, which is slightly longer than the lanthanide separation in the R_2CuO_4 phases of ca. 3.45 Å. Noting the variation in lattice parameters and cell volume with rare-earth cation (Table 4), it appears that the lanthanide ions act as spacers in the structure, affecting all of the axes isometrically.

The distorted square-planar copper coordination is certainly not unique to this structure, but the three-dimensional network formed by the CuO_4 units in RCu_2O_4 is unprecedented. Similar stacks of CuO_4 squares are found in Bi_2CuO_4 but only along one direction,[23] and in many platinum oxides,[24] for example in $CaPt_2O_4$, in which they are connected into two-dimensional layers.[25] Because the CuO_4 units of both stacks are linked via corner-sharing in a three-dimensional array, the connectivity is such that each copper atom is in contact with all others in the structure via O–Cu–O linkages. The Cu(1)–O–Cu(2) angles of

(22) VerNooy, P. D.; Stacy, A. M. *J. Solid State Chem.* **1991**, *95*, 270.
(23) Ong, E. W.; Kwei, G. H.; Robinson, R. A.; Ramakarishna, B. L.; Von Dreele, R. B. *Phys. Rev. B* **1990**, *42*, 4255.
(24) Cahen, D.; Ibers, J. A.; Mueller, M. H. *Inorg. Chem.* **1974**, *1*, 110.
(25) Schwartz, K. B.; Prewitt, C. T. *J. Chem. Phys. Sol.* **1984**, *45*, 1.

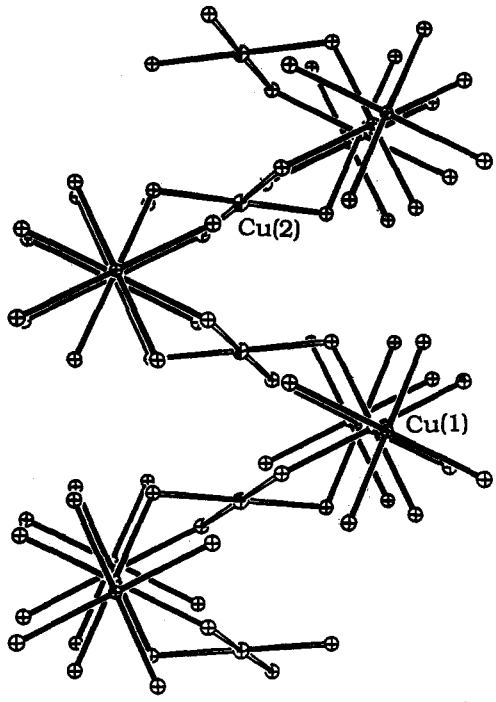

Figure 5. ORTEP diagram of the copper–oxygen connectivity in RCu_2O_4 viewed down the *c*-axis. Rare-earth atoms have been omitted for clarity, and the thermal ellipsoids represent 50% probability.

112° and 115° are substantially smaller than the angles near 180° found in the cuprates that exhibit superconductivity.

Electronic Properties. The non-uniform Cu–O bond lengths, close to what is expected for Cu^{3+} and Cu^{2+}, are an indication that the expected quarter-filled $d_{x^2-y^2}$ band is split due to electron–electron correlations. Similar splitting is also observed for the half-filled $d_{x^2-y^2}$ band in La_2CuO_4[26] and the half-filled s-band in $BaBiO_3$;[27] both of these parent materials are insulators and exhibit superconductivity when partially oxidized through doping.[2,28] It is notable that there are also two distinct Bi sites in $BaBiO_3$ with different Bi–O bond lengths, one close to that observed in oxides containing Bi^{3+} and the other close to those observed in oxides with Bi^{5+}. Although we have been unable to obtain quantitative resistivity data on our polycrystalline samples to confirm this hypothesis of a splitting of the $d_{x^2-y^2}$ band, preliminary resistivity measurements show an increase in resistivity with decreasing temperature, suggesting that $NdCu_2O_4$ is an insulator.

High-Temperature Magnetic Properties. The Curie constant and the Weiss constant were determined by a linear least-squares fit of the magnetic data obtained above ~100 K to the Curie–Weiss law for both $LaCu_2O_4$ and $NdCu_2O_4$. The fit obtained for the reciprocal molar susceptibility versus temperature for $LaCu_2O_4$ in an applied field of 5 kG is shown in Figure 6. For $SmCu_2O_4$ and $EuCu_2O_4$, the reciprocal susceptibility was not a linear function of temperature, consistent with Sm and Eu in the 3+ oxidation state; both of these ions have low-lying excited states such that the Curie–Weiss law is not applicable.

The Curie constant derived from the slope of the linear fit of the reciprocal susceptibility versus temperature is 3.11 for $LaCu_2O_4$. The spin-only value ($g = 2$) for the effective moment derived from this Curie constant is 1.61 μ_B per mole of $LaCu_2O_4$. This is consistent with one Cu^{2+} (d^9) ion per formual unit with one unpaired electron and one Cu^{3+} ion which is diamagnetic. The observed moment is slightly lower than the spin-only value for Cu^{2+} of 1.73 μ_B per mole perhaps due to covalency considerations;[29] the diamagnetism for Cu^{3+} is as expected for square-planar coordination. For $NdCu_2O_4$, the contributions to the susceptibility due to the Nd^{3+} ion ($J = 9/2$, effective moment = 3.62 μ_B per mole of Nd^{3+}) were subtracted from the total measured susceptibility to determine the contribution from the copper ions. The result of 1.89 μ_B per mole of $NdCu_2O_4$ is again consistent with the stoichiometry of one divalent copper per formula unit.

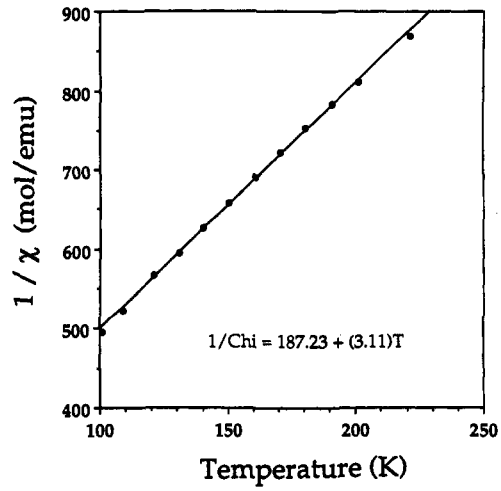

Figure 6. Reciprocal molar magnetic susceptibility versus temperature for $LaCu_2O_4$. The straight line is the best fit to the Curie–Weiss law.

The Weiss constant derived from the intercept of the linear fit of the reciprocal susceptibility versus temperature is –60 K and –44 K for $LaCu_2O_4$ and $NdCu_2O_4$, respectively; the negative Weiss constants indicate antiferromagnetic interactions. Since La^{3+} is non-magnetic, the negative Weiss constant for $LaCu_2O_4$ indicates that the antiferromagnetic ordering is associated with the *copper* sublattice.

Low-Temperature Magnetic Properties. All four of the RCu_2O_4 materials exhibit magnetic ordering at low temperature (below ca. 30 K). Magnetization measurements obtained in an applied field of 100 G for the La, Nd, Sm, and Eu phases are shown in Figure 7. In this small field, paramagnetic signals from these materials (except $NdCu_2O_4$) are barely detectable at 50 K. However, as the temperature is lowered, huge increases in the magnetizations are observed beginning at temperatures ranging from 18.0 to 28.5 K, depending on R. As the temperature is lowered further, $NdCu_2O_4$ and $SmCu_2O_4$ show a second transition to larger and smaller magnetizations at 14 and ~10 K, respectively.

The initial increase in the magnetization upon cooling for all four samples is similar, irrespective of the magnetic moment associated with R. Most notably, the magnetic ordering is observed for $LaCu_2O_4$ even though La^{3+} is non-magnetic. Therefore, we conclude that the ordering is associated with the spins on the copper ions. This is not to say that the magnetic order is completely independent of the identity of the rare earth. To the contrary, the onset temperature for the magnetic ordering is related linearly to the ionic radius of the rare-earth ion and the corresponding unit cell volume as shown in Figure 8. The observed trend is as expected for weaker interactions between copper atoms (as indicated by the lower ordering temperatures) as the distance between the copper atoms increases with increasing size of the rare-earth ions. The scaling of the onset temperature for magnetic ordering with the size and not the moment of the rare-earth ion is further evidence that the ordering just below the first transition is due to the alignment of *copper* moments (as opposed to spins on the rare-earth ions).

(26) Mattheiss, L. F. *Phys. Rev. Lett.* **1987**, *58*, 1028.
(27) Mattheiss, L. F.; Hamman, D. R. *Phys. Rev. B* **1983**, *28*, 4227.
(28) (a) Mattheiss, L. F.; Gyorgy, E. M.; Johnson, D. W., Jr. *Phys. Rev. B* **1988**, *37*, 3745. (b) Sleight, A. W.; Gillson, J. L.; Bierstedt, P. E. *Solid State Commun.* **1975**, *17*, 27.

(29) Drago, R. S. In *Physical Methods for Chemists*, 2nd ed.; Saunders College Publishing, 1992; p 484.

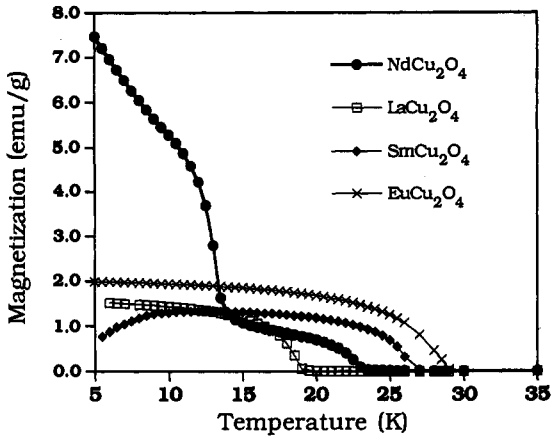

Figure 7. Gram-magnetization versus temperature obtained in a field of 100 G in the region of magnetic ordering for RCu_2O_4.

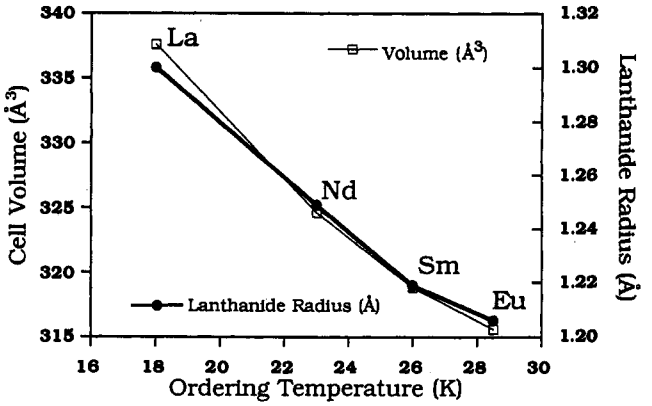

Figure 8. Magnetic ordering temperature as a function of rare-earth radius and RCu_2O_4 unit-cell volume. In $LaCu_2O_4$, the copper atoms are the farthest apart and the coupling is weakest (lowest transition temperature). Moving to smaller rare-earth ions increases the strength of the coupling and the transition temperature increases accordingly. Eight-coordinate lanthanide radii are taken from ref 36.

Measurements of the field dependence of the magnetization show saturation near 1 kG for all four samples. The saturation moments below the first transition (but above the second transition for $NdCu_2O_4$ and $SmCu_2O_4$) are ~0.13 μ_B per mole of RCu_2O_4. These were determined at 5 K for $LaCu_2O_4$ and $EuCu_2O_4$ and at 15 K for $NdCu_2O_4$ and $SmCu_2O_4$. This moment is significantly lower than the saturation moment of 1.0 μ_B per mole of RCu_2O_4 that is expected if all the spins associated with the Cu^{2+} ions are aligned parallel to the field. However, for $NdCu_2O_4$, the saturation moment of 1.1 μ_B per formula unit is observed at 2 K (below the second transition), suggesting either *ferromagnetic* alignment of the copper spins or contributions to the magnetic order from the spins on Nd^{3+}. Since the saturation moment for Nd^{3+} is 54 μ_B per mole of $NdCu_2O_4$ but the measured saturation moment is only 1.1 μ_B per mole of $NdCu_2O_4$, if the Nd^{3+} spins are ordered the predominant alignment is antiparallel.

We conclude that the overall magnetic ordering for these phases is antiferromagnetic alignment of the copper spins at low temperatures as indicated by the negative Weiss constants for $LaCu_2O_4$ and $NdCu_2O_4$. However, the increase in magnetization at low temperatures in small applied fields and the saturation moments suggest a ferromagnetic component to the ordering. We propose that the weak ferromagnetism can be attributed either to canting of the spins or to covalency effects that give rise to ferrimagnetism. These two possibilities are discussed further below.

Weak ferromagnetism has been observed in Li_2CuO_4,[30] La_2CuO_4,[31] and many orthoferrite perovskites.[32] In these materials, there is antiferromagnetic alignment of the copper moments, but the spins do not line up exactly 180° antiparallel such that there is a small ferromagnetic component. However, in contrast to what we report here for RCu_2O_4, the moments associated with the weak ferromagnetic interactions are very small, typically on the order of 10^{-3} μ_B per mole, and there is no increase in the magnetization at the onset of magnetic order because the dominant spin interactions are antiferromagnetic. Recently, Day and coworkers[33] reported a series of manganese alkylphosphate hydrates which show magnetization versus temperature plots similar to our data for RCu_2O_4. They ascribe this behavior to weak ferromagnetism brought about by a canting of the ordered Mn moments. We suggest that a model of canting of the Cu spins is also consistent with the data we have obtained for RCu_2O_4.

Another possible explanation for the co-existence of ferromagnetic and antiferromagnetic interactions is the well-known phenomenon of ferrimagnetism, where there are two separate magnetic sublattices with ferromagnetic interactions within a sublattice and antiferromagnetic interactions between the two sublattices (e.g., in Fe_3O_4). In the present case, the two sublattices could be comprised of the two sets of crystallographically distinct copper atoms. Thus far, we have assumed that the Cu(1) site is occupied by Cu^{2+} (spin = $^1/_2$) and the Cu(2) site is occupied by Cu^{3+} (spin = 0). However, since the Cu–O bonding is quite covalent, it is too simplistic to think of the two copper sites as strictly Cu^{2+} and Cu^{3+}. Partial charge (and spin) transfer from the formally divalent Cu(1) to the formally trivalent copper Cu(2) could result in a decrease in the magnitude of the spin on atoms located on the Cu(1) site and an equivalent increase at the Cu(2) site. Then ferrimagnetism can arise if the formally divalent Cu(1) atoms are ferromagnetically coupled, and the formally "trivalent" Cu(2) atoms are ferromagnetically coupled, but the two separate sublattices are coupled antiferromagnetically with respect to each other. This model is consistent with the low measured saturation moment. Neutron diffraction data are required to distinguish between these two possible models for the magnetic data.

Conclusions

We have described the synthesis, crystal structure, and magnetic properties of a new series of highly oxidized rare-earth cuprates with the formula RCu_2O_4. These phases were prepared by precipitation from molten NaOH. The structure consists of perpendicular stacks of staggered CuO_4 units that are corner-shared to form a three-dimensional copper–oxygen network. High-field susceptibility measurements on $LaCu_2O_4$ and $NdCu_2O_4$ indicate antiferromagnetic interactions dominate at temperatures below ca. 30 K. However, since all of the phases exhibit large increases in magnetization below ca. 30 K, the onset of which depends on R, we conclude that there is a significant ferromagnetic component to the ordering. Because the magnitude of this increase in magnetization is a function of the size, and not the magnetic moment of the lanthanide ion, and because the increase is observed in $LaCu_2O_4$, we ascribe the ordering to the copper sublattice.

Although the magnetic ordering mechanism is not fully understood, useful comparisons can be made between RCu_2O_4 and the cuprates that exhibit superconductivity. Cuprates with non-integral valence and an extended copper–oxygen network typically exhibit metallic conductivity, but we have found that these new phases which on average formally contain $Cu^{2.5+}$ ($d_{x^2-y^2}$ band quarter-filled) are a special case, analogous to the cuprates with Cu^{2+} ($d_{x^2-y^2}$ band half-filled); both classes of cuprates are non-metallic and exhibit magnetic ordering. We conclude that the decrease in the Cu–O–Cu bond angle from 180° in the layered

(30) Sapiña, F.; Rodríguez-Carvajal, J.; Sanchis, M. J.; Ibáñez, R.; Beltrán, A.; Beltrán, D. *J. Solid State Chem.* **1990**, *74*, 799.
(31) Thio, T. et. al. *Phys. Rev. B* **1988**, *38*, 905.
(32) Goodenough, J. B.; Longo, J. M. In *Landolt-Bornstein New Series*; Springer-Verlag: New York, 1970; Vol. 4, Part a, pp 126–314.
(33) Carling, S. G.; Day, P.; Visser, D.; Kremer, R. K. *J. Solid State Chem.* **1993**, *106*, 111–119.

cuprates to near 115° in RCu_2O_4 results in a change from antiferromagnetic coupling to ferromagnetic coupling between copper moments, although a competition between the two interactions remains. Furthermore, while the coupling between the copper moments in RCu_2O_4 is influenced by the neighboring magnetic lanthanide ions (Nd and Sm), superconductivity is unaffected by the magnetic moment associated with the rare-earth ions in $RBa_2Cu_3O_7$[34] and $R_{2-x}Ce_xCuO_4$.[35] Therefore, with this new class of compounds, there is a special opportunity to probe magnetic interactions between copper moments, as well as between copper and rare-earth moments in an extended oxide structure.

Acknowledgment. This work was supported by the National Science Foundation (Grant DMR-9102492) and a National Science Foundation Faculty Award for Women Scientists and Engineers (Grant DMR-9023600). We thank K. Schwartz of Raychem Corp. for collecting some of the X-ray diffraction data, J. Donovan of the Geology department at U. C. Berkeley for performing the microprobe analyses, and M. Fendorf for the micrograph shown in Figure 1. A.M.S. thanks the Alfred P. Sloan Foundation and the Camille and Henry Dreyfus Foundation for their support.

(34) (a) Zao, F.; Patton, B. R.; Cox, D. L.; Lee, S. I.; Song, Y.; Golben, J. P.; Chen, X. D.; Lee, S. Y.; Cao, Y.; Lu, Y.; Gains, J. R.; Garland, J. C.; Epstein, A. J. *Phys. Rev. B* **1987**, *36*, 3603. (b) Hor, P. H.; Meng, R. L.; Wang, Y. Q.; Gao, L.; Huang, Z. L.; Bechtold, J.; Forster, K.; Chu, C. W. *Phys. Rev. Lett.* **1987**, *58*, 1891.

(35) Tokura, Y.; Takagi, H.; Uchida, S. *Nature* **1989**, *337*, 345–6.

(36) Shannon, R. D. *Acta Crystallogr.* **1976**, *A32*, 751.